

000  
001  
002  
003  
004  
005  
006  
007  
008  
009  
010  
011  
012  
013  
014  
015  
016  
017  
018  
019  
020  
021  
022  
023  
024  
025  
026  
027  
028  
029  
030  
031  
032  
033  
034  
035  
036  
037  
038  
039  
040  
041  
042  
043  
044

# HF-FCN: Hierarchically Fused Fully Convolutional Network for Robust Building Extraction

Anonymous ACCV 2016 submission

Paper ID 663

**Abstract.** Currently, automatic building extraction from remote sensing images plays an important role in a diverse range of applications. However, it is significantly challenging to extract arbitrary-size buildings with large variant appearances or occlusions. To tackle these problems, we propose a robust system employing a novel hierarchically fused fully convolutional network (HF-FCN), which effectively integrates the information generated from a group of neurons with multi-scale receptive fields. Our architecture can take whole aerial images as inputs without warping or cropping and output building map directly. The experiment results tested on a publicly available aerial imagery dataset prove that our proposed methodology surpass the performance of state-of-the-art method and significantly reduce time cost.

## 1 Introduction

With the rapid development of remote sensing technologies and popularization of geospatial related commercial softwares, very high resolution satellite images are easily accessible. These valuable data provide a huge fuel for interpreting real terrestrial scenes. The building rooftop is one of the most important type of terrestrial objects because it is essential for a wide range of technologies, such as, urban planning, automated map making, 3D city modelling, disaster assessment, military reconnaissance, etc. However, it is very costly and time-consuming to manually delineate the footprint of buildings even for human experts.

In recent decades, many researchers have made massive attempts to extract buildings automatically. Much of the past works define criteria according to the particular characteristics of rooftop, such as, polygonal boundary [1–4], homogeneous color or texture [5], surrounding shadow [6–9], and their combinations [10, 11]. However, such approaches are weakly capable of handling real-world data because hand-coded rules or probability models learned from small samples are much dependent on data. For example, they assume that profile of buildings is polygon while the shape of stadiums always is circle or oval. For the sake of deploying a practical building extraction system, Mnih [12] created a huge publicly dataset including large-scale aerial images and corresponding human-labeled maps, and proposed a patch-based convolutional neural network to extract location of objects automatically. Based on Mnih’s work, Saito *et al.*

CONFIDENTIAL REVIEW COPY. DO NOT DISTRIBUTE.

2 ACCV-16 submission ID 663

[13] improved the performance further by developing two effective techniques. Though these methods achieve high performance, they still have limited ability to deal with two often appearing cases: (1) Buildings are occluded by shadows or trees. (2) Buildings possess moderately variant appearances.

Mapping buildings from aerial image is essentially a problem of semantic segmentation. Recent work suggests a number of methods in processing natural images. Long *et al.* [14] firstly proposed a effective architecture for semantic image segmentation, namely, fully convolutional network (FCN). Chen *et al.* [15] presented a system which combines the responses at the final convolutional layer with a fully connected conditional random field (CRF). The system is able to localize segment boundaries at a quite high level of accuracy. Zheng *et al.* [16] introduced an end-to-end network which integrates CRF with CNNs to avoid off-line post-processing for object delineation. Noh *et al.* [17] applied a deconvolution network to each proposal in a input image, and construct the final semantic segmentation map by combining the results from all proposals in a simple manner.

Although these methods show promise in segmenting natural images, they have components not suited for building extraction. Firstly, buildings are frequently occluded by shadows or trees (see Fig.1 (a)). It is challengable to delineate building boundaries even for human experts. Though some literatures [15, 16] achieve excellent performance in processing boundary of natural image, neither of them reported that they have strong ability in handling occlusions. Secondly, buildings have significantly variant appearances even in a single one. (see Fig.1 (b)). Moreover, a number of buildings are very close to the plot on the ground or road (see Fig.1 (c)). Based on our observation, there are few such samples emerge in PASACAL VOC 2012 [18] dataset. Last but not the least, the size of objects in a remote sensing image is in a wide range. For example, some images include a large number of tiny buildings (see Fig.1 (d)) and some ones are composed of moderate quantity of small-scale rooftops and a few large-scale rooftops. On account of low resolution (one-eighth resolution of input image) of output from [14], precise structures are sacrificed severely. Noh *et al.* [17] claimed it handles objects in multiple scales, but it only suitable to multi-classes object segmentation.

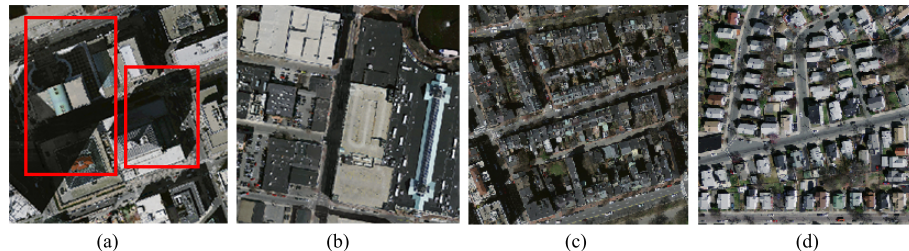


**Fig. 1.** Examples of aerial image. (a) Occlusions (shown in red rectangle). (b) Variant appearances. (c) Low contrast. (d) A large number of tiny buildings.

090 Here, we present a robust building extraction system by developing a hi-  
091 erarchically fused fully convolutional network (HF-FCN) trained on a publicly  
092 available large aerial imagery dataset [12]. In our architecture (HF-FCN), we  
093 design a new scheme to integrate multi-level semantic information generated  
094 from convolutional layers with a group of incremental receptive fields. Incre-  
095 mental sized receptive fields are able to capture context information in different  
096 neighbourhood sizes. Therefore, it is more effective to handling buildings with  
097 arbitrary sizes, variant appearances or occlusions. Compared with [12, 13], over-  
098 lapped cropping and model averaging are not required for HF-FCN. It takes  
099 whole images as inputs, and directly outputs segmentation maps by one pass of  
100 forward propagation. Hence, our system decreases the computation complexity  
101 significantly. In conclusion, our contributions include two aspects: (1) A new  
102 architecture is developed for building extraction, which has a strong ability in  
103 processing appearance variations, varying sizes and occlusions. Meanwhile, the  
104 overall accuracy also exceeds state-of-the-art [13]. (2) Our approach leads to a  
105 notable reduction of computation cost compared with traditional solutions.  
106

107 The rest of this article is organized as follows. In Section 2, we summarize  
108 main methods for building extraction. Section 3 provides details of our neural  
109 network architecture and formulation of building extraction problem. Section 4  
110 introduces the dataset and training strategies of our proposed network, and then  
111 we compare our results with two patch-based methods using the three types of  
112 criteria. In Section 5, we discuss the experimental results and summarize whole  
113 article.

## 114 2 Related Work 115

116 In previous literatures, one popular way of extracting buildings is employing their  
117 shape information. It is observed that rooftops have more regular shapes, which  
118 usually are rectangular or combinations of several rectangles. Several studies [1–  
119 4] exploited a graph-based search to establish a set of rooftop hypotheses through  
120 examining the relationships of lines and line intersections, and then removed the  
121 fake hypotheses using a series of criteria. Cote and Saeedi [5] generated rooftop  
122 outline from selected corners in multiple color and color-invariance spaces, fur-  
123 ther refined to fit the best possible boundaries through level-set curve evolution.  
124 Though these geometric primitives based methods achieve good performance  
125 in high contrast remote sensing imagery, they suffer from three shortcomings.  
126 Firstly, they lack the ability of detecting arbitrarily shaped building rooftop.  
127 Secondly, they fail to extract credible geometric features in buildings with in-  
128 homogeneous color distribution or low contrast with surroundings. Thirdly, it is  
129 time-consuming to process large-scale scenes because of their high computational  
130 complexity.

131 Apart from using shape information, spectral information is a distinctive  
132 feature for terrestrial object extraction. For instance, shadows are commonly  
133 dark grey or black, vegetations are usually green or yellow with particular tex-  
134 tures, and main roads are dim gray in most cases. According to these prior

CONFIDENTIAL REVIEW COPY. DO NOT DISTRIBUTE.

4 ACCV-16 submission ID 663

knowledge, Ghaffarian *et al.* [19] split aerial scenes into three components (respectively, shadows and the vegetation, roads and the bare soil, buildings) using a group of manually established rules. Afterwards, a purposive fast independent component analysis (PFastICA) technique is employed to separate building area from remote sensing image. However, their results are significantly sensitive to parameter choice. A feasible alternative strategy is to learn the appearance representation using supervised learning algorithm. A number of authors [8–10, 20] designed a similar framework. Firstly, an aerial image is divided into superpixels using a certain over-segmentation algorithm. Secondly, hand-crafted features, such as, color histograms or local binary patterns (LBP), are extracted from each over-segmented regions. Finally, each region is classified using machine learning tools and a gallery of training descriptors. Because it's inevitable for machine learning method to mislabel regions with similar appearance, additional information is utilized to refine previous results. Ngo *et al.* [9] removed false rooftops using a assumption that buildings are surrounded by shadows because of illumination. Baluyan et al. [10] devised a “histogram method” to detect missed rooftops. Li *et al.* [11] selected probable rooftops after pruning out blobs using shadows, light direction, a series of shape criteria, and then these rooftops is refined by high order conditional random field. The drawbacks of these algorithms are threefold. (1) It is problematic to recognize a over-segmented region as part of buildings because terrestrial objects have huge variant appearances in real aerial scene. (2) Hand-craft features are sensitive to input data, therefore, it is not robust to process large-scale remote sensing images. (3) Additional information is unreliable. For instance, some low buildings have no shadow in its neighbourhood, and some buildings have unique structures which are not satisfied to hand-coded criteria.

As mentioned above, traditional methods are weakly capable of adapting to real scenes with huge variant appearances, occlusions or low contrast. Our method does not design image features manually, on the contrary, building features are directly learned from a mass of real data using deep neural networks. Therefore, our algorithm is more robust to extract buildings in real scenes. Mnih, a pioneer, presented a patch-based framework for learning to label aerial images [12]. A neural network architecture is carefully designed for predicting buildings in aerial imagery, and the output of this network is processed by conditional random fields (CRFs). Satito *et al.* [13] improved Mnih’s networks for extracting multiple kinds of objects simultaneously, two techniques consisting of model averaging with spatial displacement (MA) and channel-wise inhibited softmax (CIS) are introduced to enhance the performance. However, these methods need to crop test image into a fixed size, which not only increases the time cost, but also breaks the integrity of buildings. Our system takes whole images as inputs without overlapped cropping or wrapping and directly outputs labelling images. It is much beneficial to preserve the whole structure of buildings and shorten computation time.

180    **3 System Overview**

181  
182    In this section, we introduce a hierarchically fused fully convolutional network  
183    (HF-FCN) for extracting rooftops, and then formulate our problem and loss  
184    function.

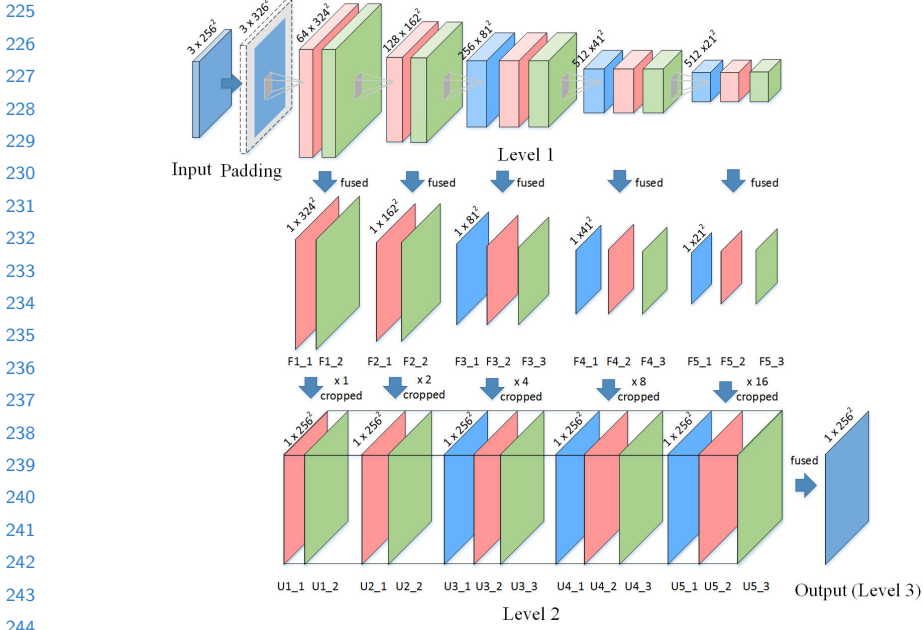
185    **3.1 Network Architecture**

186    We design our network based on VGG16 Net [21] and make some modifications.  
187    The reasons for choose VGG16 Net are two-fold: (1) It has great depth (16  
188    convolutional layers), and multiple stages (five 2-stride down-sampling layers).  
189    We can acquire enough multi-level information from different stages and convolu-  
190    tional layers. (2) Network parameters pre-trained on very large image dataset  
191    (ImageNet) are helpful for initializing our network because our aerial data is  
192    essentially optical imagery. The modifications are listed as follows: (1) Two fully  
193    connected layer  $fc_6$ ,  $fc_7$  and fifth pooling layer are cut, because they are at 1/32  
194    of input resolution with the consequence that the interpolated prediction map  
195    will be too fuzzy to utilize. Meanwhile, the number of neurons in  $fc_6$ ,  $fc_7$  is too  
196    large to cost intensive computation. (2) Feature maps from each convolutional  
197    layer in trimmed VGG16 Net (denote as Level 1) are fed into a convolutional  
198    layer with a filter of kernel size of  $1 \times 1$ . The outputs of these convolutional layers  
199    are upsampled and cropped to the same size of input image (denote as Level  
200    2). Upsampling is implemented via deconvolution which is initialized by bilinear  
201    interpolation. Finally, all the feature maps in Level 2 are stacked and put into  
202    a convolutional layer with a filter of kernel size of  $1 \times 1$  to yield final predicted  
203    map (denote as Level 3). (3) The size of feature map in last stage of Level 1 is  
204    1/16 of input image, it is too small to use. Thus, we apply a popular trick that  
205    input images are padded with all-zero band to enlarge the size of feature maps.  
206    Our architecture is shown in Fig. 2.

207    **Table 1.** The receptive field (rf) and stride size of Level 2 in our architecture.

| layer   | F1_1 | F1_2 | F2_1 | F2_2 | F3_1 | F3_2 | F3_3 | F4_1 | F4_2 | F4_3 | F5_1 | F5_2 | F5_3 |
|---------|------|------|------|------|------|------|------|------|------|------|------|------|------|
| rf size | 3    | 5    | 10   | 14   | 24   | 32   | 40   | 60   | 76   | 92   | 124  | 164  | 196  |
| stride  | 1    | 1    | 2    | 2    | 4    | 4    | 4    | 8    | 8    | 8    | 16   | 16   | 16   |

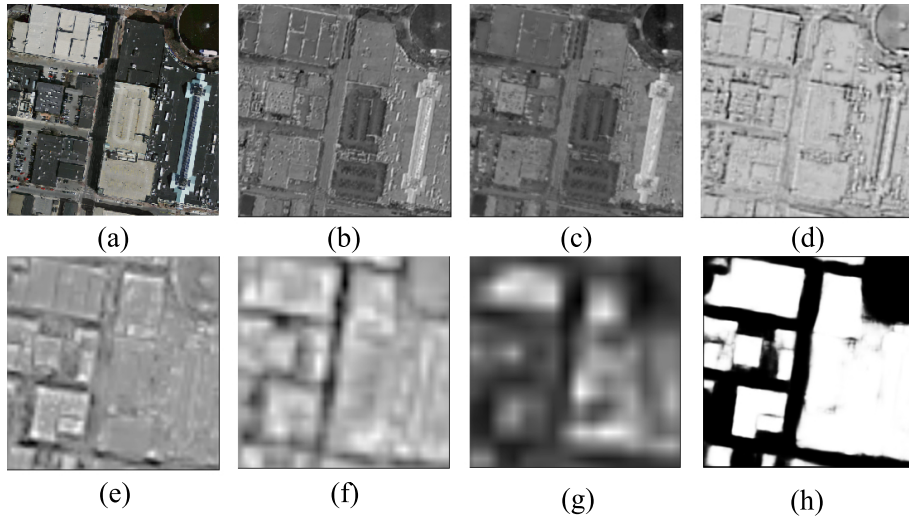
208  
209  
210  
211    In Level 2 of our architecture, feature maps with increasing receptive field  
212    (see Table 1) capture local information in different neighbourhood sizes and at d-  
213    ifferent semantic levels. Therefore, if we integrate all these information together,  
214    it is helpful for extracting buildings with variant appearances or occlusions. We  
215    take a concrete instance to show how HF-FCN works for such cases. In this case,  
216    U1\_1 with small receptive field generates fine spatial resolution and responds  
217    to low level features like edges and corners (see Fig. 3(b)). U1\_2 functions like  
218    over-segmentation algorithm to grouping pixels with similar color or texture in-  
219    to a subregion (see Fig. 3(c)). In U2\_1, color information is disappear, shape  
220  
221  
222  
223  
224

**Fig. 2.** Our network architecture.

information is augmented (see Fig. 3(d)). In U3\_3, it is surprised that regions with significantly varying appearance are merged into a integrated building by considering some unknown high level features (see Fig. 3(e)). In U4\_2 and U5\_2, our network learned strong semantic knowledge to distinguish dark rooftops with dim shadows and dark-green water (see Fig. 3(f)(g)). In Level 3, we show that HF-FCN obtains reliable prediction by combining multi-level semantic information and spatial information (see Fig. 3(h)).

### 3.2 Formulation

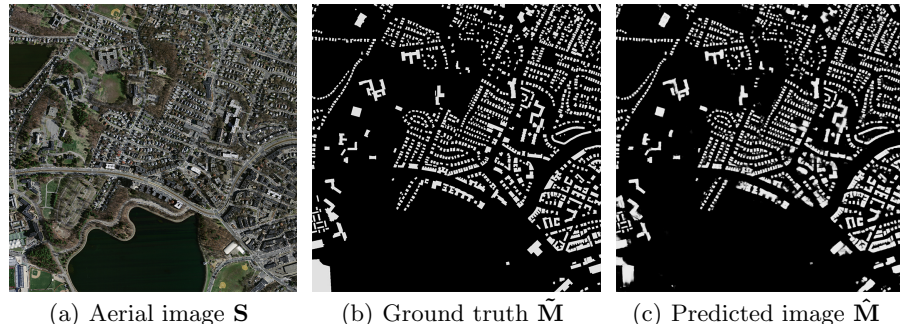
Our goal is to predict labelling image  $\hat{\mathbf{M}}$  from a input aerial image  $\mathbf{S}$ . We directly learn a mapping from raw pixels in  $\mathbf{S}$  to a true label image  $\hat{\mathbf{M}}$  by training the whole network. Fig. 4 shows an example of  $\mathbf{S}$ ,  $\hat{\mathbf{M}}$ ,  $\tilde{\mathbf{M}}$ . Here we formulate our approach for building extraction. We denote our input training data set by  $\mathbf{I} = \{(\mathbf{S}_n, \tilde{\mathbf{M}}_n), n = 1, \dots, |\mathbf{S}_n|\}$ , where sample  $\mathbf{S}_n = \{s_j^{(n)}, j = 1, \dots, |\mathbf{S}_n|\}$  denotes the raw input image and  $\tilde{\mathbf{M}}_n = \{\tilde{m}_j^{(n)}, j = 1, \dots, |\mathbf{S}_n|\}$ ,  $\tilde{m}_j^{(n)} \in \{0, 1\}$  denotes the corresponding ground truth binary labelling map for satellite image  $\mathbf{S}_n$ . Taking account of each image holistically and independently, thus, we adopt the subscript  $n$  for notational simplicity. Our goal is to have a network that learns features from which it is possible to produce building maps approaching the ground truth. In our image-to-image training, the loss function is computed



**Fig. 3.** (a) Input aerial image. (b - g) Feature maps generated from U1\_1, U1\_2, U2\_1, U3\_3, U4\_2, U5\_2, respectively. (h) Predicted labelling map.

over all pixels in a training image  $\mathbf{S} = \{s_j, j = 1, \dots, |\mathbf{S}|\}$  and building map  $\tilde{\mathbf{M}} = \{\tilde{m}_j, j = 1, \dots, |\mathbf{S}|\}, \tilde{m}_j \in \{0, 1\}$ . For simplicity, we denote the collection of all standard network layer parameters as  $\mathbf{W}$ . For each pixel  $j$  in a training image, the possibility that assigns it to building is denoted as  $\hat{m}_j = Pr(\tilde{m}_j = 1 | \mathbf{S}; \mathbf{W})$ . the definition of sigmoid cross-entropy loss function is shown in Eq (1).

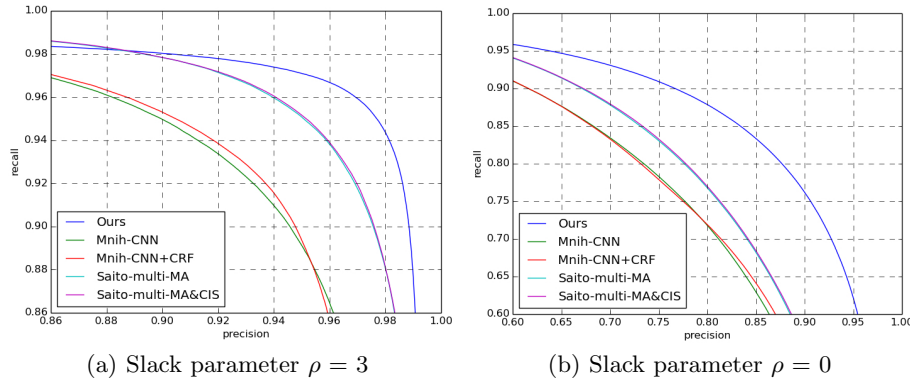
$$\mathcal{L} = -\frac{1}{|\mathbf{S}|} \sum_{j \in \mathbf{S}} [\tilde{m}_j \log \hat{m}_j + (1 - \tilde{m}_j) \log (1 - \hat{m}_j)] \quad (1)$$



**Fig. 4.** An example of the resulting predicted image.

315 **4 Experiments** 315  
316317 In this section, we introduce our detailed implementation and report the perfor- 317  
318 mance of our proposed algorithm. 318  
319320 **4.1 Dataset** 320  
321322 In our experiments, we use Massachusetts Buildings Dataset (*Mass. Buildings*) 322  
323 proposed by Mnih [12] and publicly available on website [http://www.cs.toronto.](http://www.cs.toronto.edu/~vmmnih/data/) 323  
324 The dataset consists of 151 aerial images of the Boston area, 324  
325 with each of the images being  $1500 \times 1500$  pixels for an area of 2.25 square k- 325  
326 ilometers. Hence, the entire dataset covers roughly 340 square kilometers. The 326  
327 data is split into a training set of 137 images, a test set of 10 images and a vali- 327  
328 dation set of 4 images. To train the network, we create image tiles for train and 328  
329 validation by means of cropping entire image using a sliding window with size 329  
330 of  $256 \times 256$  pixels and stride of 64 pixels. When scanning the whole dataset, im- 330  
331 age tiles which include more than 160 white pixels are removed. After scanning, 331  
332 train and validation dataset include 75938 tiles and 2500 tiles with corresponding 332  
333 building masks. For testing, we use ten  $1500 \times 1500$  entire images covering area 333  
334 excluded from the training data. In our experiments, we find that it is benefit 334  
335 to improving prediction performance by means of scaling the intensity of input 335  
336 image into range of [0,1]. 336  
337338 **4.2 Training Settings** 338  
339340 The implementation of our network is based on the publicly available *Caffe* [22] 340  
341 Library. HF-FCN is fine-tuned from an initialization with the pre-trained VGG16 341  
342 Net model and trained in an end-to-end manner. It is trained using stochastic 342  
343 gradient descent with the following hyper-parameters, including mini-batch size 343  
344 (18), initial learning rate ( $10^{-5}$ ), learning rate is divided by 10 for each 5000 344  
345 iterations, momentum (0.9), weight decay (0.02), clip\_gradients (10000), number 345  
346 of training iterations (12000). We find that learned deconvolutions provide no 346  
347 noticeable improvements in our experiments, therefore, lr\_mult is set to zero for 347  
348 all deconvolutional layers. Additionally, except that the pad of first convolutional 348  
349 layer is set to 35, others are set to 1 as the same as VGG16 Net. It takes about 349  
350 six hours to train a network on a single NVIDIA Titan 12GB GPU. 350  
351352 **4.3 Results** 352  
353354 To show the effectiveness of HF-FCN, we train and test our network on *Mass.* 354  
355 *Buildings*. In order to comparing our results with previous works [12, 13], we use 355  
356 three metrics to evaluate our results: (1) relaxed precision and recall scores ( $\rho$  356  
357 = 3). (2) relaxed precision and recall scores ( $\rho$  = 0). (3) time cost. The relaxed 357  
358 precision is defined as the fraction of detected pixels that are within  $\rho$  pixels 358  
359 of a detected pixel, while the relaxed recall is defined as the fraction of true 359

360 pixels that are within  $\rho$  pixels of a detected pixel. In one of our experiments,  
 361 the slack parameter  $\rho$  is set to 3, which is the same value as used in [12, 13].  
 362 Compared relaxed precision-recall curves are shown in Fig. 5(a). In order to  
 363 evaluate our results more strictly, we set slack parameter  $\rho$  as 0, that is to say,  
 364 it becomes a standard precision and recall scores. Compared standard precision-  
 365 recall curves are shown in Fig. 5(b). Additionally, time cost is another important  
 366 index to evaluate system performance. We calculate the mean time of processing  
 367 ten test images in the same computer using the same program. Table 2 shows  
 368 that our method is able to not only significantly improve the performance, but  
 369 dramatically decrease the time cost.  
 370

**Fig. 5.** Two relaxed precision-recall curves**Table 2.** Performance is compared with [12, 13]. Recall here means recall at breakeven points. Time is computed in the same computer with a single NVIDIA Titan 12GB GPU.

|                         | Recall ( $\rho = 3$ ) | Recall ( $\rho = 0$ ) | Time (s)    |
|-------------------------|-----------------------|-----------------------|-------------|
| Mnih-CNN [12]           | 0.9271                | 0.7661                | 8.70        |
| Mnih-CNN+CRF [12]       | 0.9282                | 0.7638                | 26.60       |
| Saito-multi-MA [13]     | 0.9503                | 0.7873                | 67.72       |
| Saito-multi-MA&CIS [13] | 0.9509                | 0.7872                | 67.84       |
| Ours (HF-FCN)           | <b>0.9643</b>         | <b>0.8424</b>         | <b>1.07</b> |

400 To prove our network having strong ability in extracting buildings with vari-  
 401 ant appearances, arbitrary sizes, occlusions, we perform further evaluation. We  
 402 crop seven  $256 \times 256$  image patches that have buildings with variant appear-  
 403 ances or occlusions from test image of *Mass. Buildings*. And then, we directly  
 404 crop corresponding predictions from predicted images generated by three models

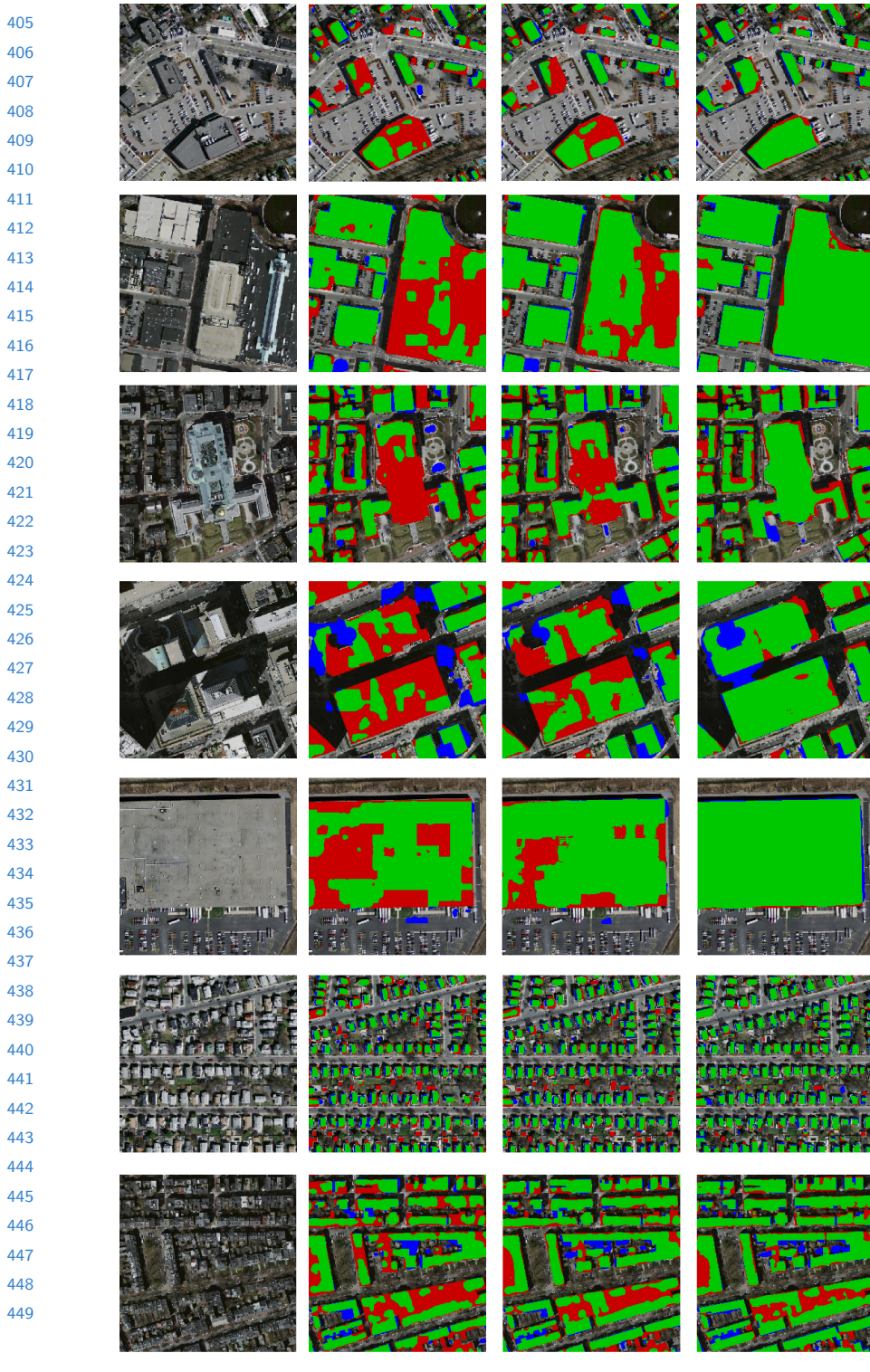


**Fig. 6.** (a) Input images. (b) Results of Mnih-CNN+CRF [12]. (c) Results of Saito-multi-MA&CIS [13]. (d) Our results. Correct results (TP) are shown in green, false positives (FP) are shown in blue, and false negatives (FN) are shown in red.

(Mnih-CNN+CRF [12], Saito-multi-MA&CIS [13] and ours). Here, we binarize the probability map using a threshold of 0.5. Seven groups of example are shown in Fig. 6. In addition, Table 3 shows the resulting recalls at breakeven points of standard precision recall curve for each patches.

Table 3. Recall at selected region of the test images

| Image ID                | 01           | 02           | 03           | 04           | 05           | 06           | 07           | mean         |
|-------------------------|--------------|--------------|--------------|--------------|--------------|--------------|--------------|--------------|
| Mnih-CNN+CRF [12]       | 0.784        | 0.869        | 0.769        | 0.653        | 0.893        | 0.764        | 0.800        | 0.784        |
| Saito-multi-MA&CIS [13] | 0.773        | 0.915        | 0.857        | 0.789        | 0.945        | 0.773        | 0.830        | 0.851        |
| Ours (HF-FCN)           | <b>0.874</b> | <b>0.964</b> | <b>0.899</b> | <b>0.901</b> | <b>0.986</b> | <b>0.840</b> | <b>0.851</b> | <b>0.911</b> |

## 5 Conclusions

In this article, we propose a improved fully convolutional network which is strongly capable of extracting buildings with arbitrary sizes, variant appearances or occlusions without any post-processing. Meanwhile, it further improves the overall accuracy. The network can take arbitrary-size image as input as long as GPU memory allowed. Compared with patch-based methods, there is no need to label a whole image by cropping the image into small patches. As consequence, inconsistant border caused by cropped would not occurred in our system. Though some effective techniques, such as model average and conditional random field, can improve the performance further, time cost is increased by several times. While in our system, elapsed time is tremendously decreased. On the other hand, we demonstrate that our network is generally adapt to various types of aerial scenes selected from real-world data. Furthermore, our architecture can be easily extended to extract multi-objects in remote sensing imagery. Consequently, we believe that our technique potentially provides a generic solution to understand complex aerial scenes.

## References

1. Noronha, S., Nevatia, R.: Detection and modeling of buildings from multiple aerial images. *Pattern Analysis and Machine Intelligence, IEEE Transactions on* **23** (2001) 501–518
2. Nosrati, M.S., Saeedi, P.: A novel approach for polygonal rooftop detection in satellite/aerial imageries. In: *Image Processing (ICIP), 2009 16th IEEE International Conference on*, IEEE (2009) 1709–1712
3. Izadi, M., Saeedi, P.: Three-dimensional polygonal building model estimation from single satellite images. *Geoscience and Remote Sensing, IEEE Transactions on* **50** (2012) 2254–2272

CONFIDENTIAL REVIEW COPY. DO NOT DISTRIBUTE.

12 ACCV-16 submission ID 663

- 495 4. Wang, J., Yang, X., Qin, X., Ye, X., Qin, Q.: An efficient approach for automatic  
496 rectangular building extraction from very high resolution optical satellite imagery.  
497 Geoscience and Remote Sensing Letters, IEEE **12** (2015) 487–491  
498 5. Cote, M., Saeedi, P.: Automatic rooftop extraction in nadir aerial imagery of  
499 suburban regions using corners and variational level set evolution. Geoscience and  
500 Remote Sensing, IEEE Transactions on **51** (2013) 313–328  
501 6. Sirmacek, B., Unsalan, C.: Building detection from aerial images using invariant  
502 color features and shadow information. In: International Symposium on Computer  
503 and Information Sciences. (2008) 1–5  
504 7. Ok, A.O., Senaras, C., Yuksel, B.: Automated detection of arbitrarily shaped  
505 buildings in complex environments from monocular vhr optical satellite imagery.  
506 Geoscience and Remote Sensing, IEEE Transactions on **51** (2013) 1701–1717  
507 8. Chen, D., Shang, S., Wu, C.: Shadow-based building detection and segmentation  
508 in high-resolution remote sensing image. Journal of Multimedia **9** (2014) 181–188  
509 9. Ngo, T.T., Collet, C., Mazet, V.: (Automatic rectangular building detection from  
510 vhr aerial imagery using shadow and image segmentation)  
511 10. Baluyan, H., Joshi, B., Al Hinai, A., Woon, W.L.: Novel approach for rooftop  
512 detection using support vector machine. ISRN Machine Vision **2013** (2013)  
513 11. Li, E., Femiani, J., Xu, S., Zhang, X., Wonka, P.: Robust rooftop extraction from  
514 visible band images using higher order crf. Geoscience and Remote Sensing, IEEE  
515 Transactions on **53** (2015) 4483–4495  
516 12. Mnih, V.: Machine learning for aerial image labeling. Doctoral (2013)  
517 13. Saito, S., Yamashita, Y., Aoki, Y.: Multiple object extraction from aerial imagery  
518 with convolutional neural networks. Journal of Imaging Science & Technology **60**  
519 (2016)  
520 14. Long, J., Shelhamer, E., Darrell, T.: Fully convolutional networks for semantic  
521 segmentation. Computer Science **79** (2014) 1337–1342  
522 15. Chen, L.C., Papandreou, G., Kokkinos, I., Murphy, K., Yuille, A.L.: Semantic  
523 image segmentation with deep convolutional nets and fully connected crfs. In:  
524 ICLR. (2015)  
525 16. Zheng, S., Jayasumana, S., Romera-Paredes, B., Vineet, V.: Conditional random  
526 fields as recurrent neural networks. (2015) 1529–1537  
527 17. Noh, H., Hong, S., Han, B.: Learning deconvolution network for semantic segmen-  
528 tation. (2015)  
529 18. Everingham, M., Van Gool, L., Williams, C.K.I., Winn, J., Zisserman, A.: The  
530 PASCAL Visual Object Classes Challenge 2012 (VOC2012) Results.  
531 ([http://www.pascal-  
532 network.org/challenges/VOC/voc2012/workshop/index.html](http://www.pascal-network.org/challenges/VOC/voc2012/workshop/index.html))  
533 19. Ghaffarian, S., Ghaffarian, S.: Automatic building detection based on purposive  
534 fastica (pfica) algorithm using monocular high resolution google earth images. IS-  
535 PRS Journal of Photogrammetry and Remote Sensing **97** (2014) 152–159  
536 20. Dornaika, F., Moujahid, A., Bosaghzadeh, A., El Merabet, Y., Ruichek, Y.: Object  
537 classification using hybrid holistic descriptors: Application to building detection in  
538 aerial orthophotos. Polibits (2015) 11–17  
539 21. Simonyan, K., Zisserman, A.: Very deep convolutional networks for large-scale  
image recognition. Eprint Arxiv (2014)  
22. Jia, Y., Shelhamer, E., Donahue, J., Karayev, S., Long, J., Girshick, R., Guadarrama,  
S., Darrell, T.: Caffe: Convolutional architecture for fast feature embedding.  
Eprint Arxiv (2014) 675–678